ChemComm

Accepted Manuscript

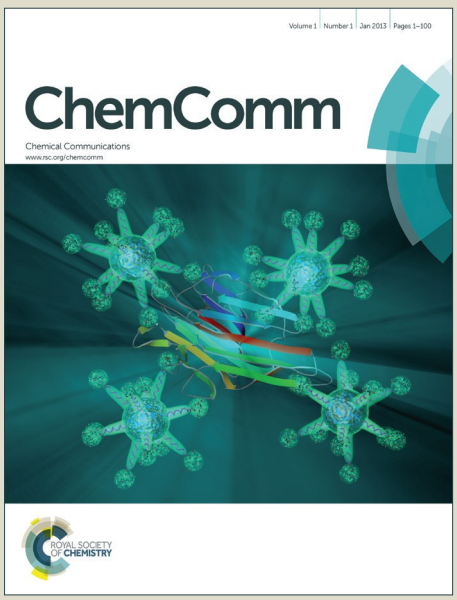

ROYAL SOCIETY OF CHEMISTRY

www.rsc.org/chemcomm

ChemComm

COMMUNICATION

Bayberry-like ZnO/MFI Zeolite as High Performance Methanol-to-aromatics Catalyst

Received 00th January 20xx,
Accepted 00th January 20xx

DOI: 10.1039/x0xx00000x

www.rsc.org/

Ning Wang, Weizhong Qian, Kui Shen, Chang Su and Fei Wei

Unique bayberry-like MFI zeolite are synthesized through quasi-solid-state crystallization approach. This hierarchical zeolite structure has relatively thick shell, densely grown nanocrystals with ordered packed channel, high mechanical stability, high surface area and low Si/Al ratio. Its catalytic efficiency for methanol-to-aromatics is significantly higher than that of conventional MFI zeolite.

Although aromatics, very important basic chemicals, were mainly produced from oil-based route to this date, the gradual depletion of oil reserve resulted in the sustainably tight supply and high cost of aromatics. In the past two decades, the route of converting methanol to aromatics (MTA) has received intensive attention considering methanol was easily available from wide resources such as coal, natural gas, shale gas and biomasses.[1,2] High catalytic conversion with desirable and high product selectivity will reduce the highly energy-consumed separation step and, consequently, contribute effectively to the clean energy issue considering the significantly suppression release of CO_x or NO_x. Compared to nanosized zeolite, microsized zeolite gave a higher selectivity of benzene (B), toluene (T), xylene (X) from methanol, but suffered from the rapid deactivation of the catalyst due to the diffusion limitation of intermediate product with large size in zeolite channel.[3] Nanosized MFI zeolite had long catalytic life, due to the fact that the dimensional reduction in size enhanced the diffusion.[4,5] But conventional fine nanozeolite powder can cause an overhigh pressure drop in reactor bed and was very difficult to filtrate, as well as the production of waste water in large quantities.[6-8] To this date, it remained a great challenge to prepare a rational structure with high acidic strength and good mechanical stability to combine both advantages and to avoid both disadvantages of micro- and nano- crystals.

Herein, we propose a macroscopic bayberry-like MFI zeolite structure with micrometer-thick shell and numerous zeolite nanowires (NWs) vertically grown on them with good alignment. Such novel structure was prepared by an *in-situ* transforming solid mesoporous silica (MS) spheres in high-temperature steam (Fig. S1). By modulating the initial seed density and the amount of $NaAlO_2$ minerializer, for the first time, we were not only able to control the orientation and the density of zeolite NWs on the shell, but also able to obtain MFI zeolite with high acidic strength (Si/Al ratio is 8−25, far lower than that (>30) in previous works).[8] As a result, this structure with high amount of acids and good mechanical strength exhibited higher product distribution and much longer lifetime than that of conventional zeolite catalyst in methanol to aromatics. This result provides a new insight on the fabrication of tailored MFI zeolite structure toward many other applications.

The starting MS spheres with uniform size of ~15 μm (Fig. 1a) had a relatively rough surface and many tiny pits (Fig. 1b). These spheres with surface area of 48.1 m^2/g and the mesopores of 7−27 nm in large amounts were mainly the amorphous phase, reflected by the peak centered at around 22° in XRD pattern (Fig. S2).[9-11]

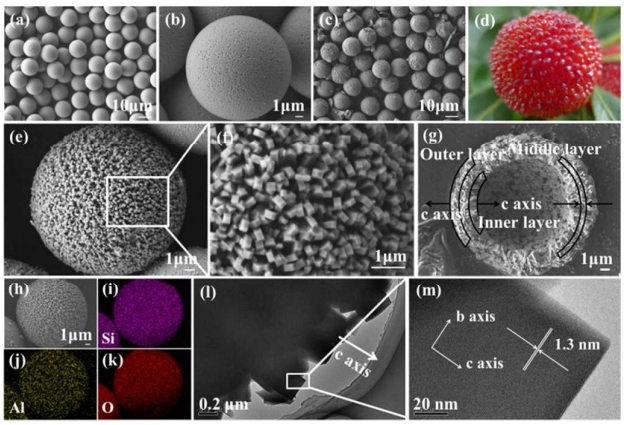

Fig. 1 SEM images of (a and b) MS spheres, (c,e and f) bayberry-like MFI zeolite, (g) crushed MFI zeolite; (d) Photographs of bayberry; (h-k) EDX element mapping; (l and m) TEM images of bayberry-like MFI zeolite.

Beijing Key Laboratory of Green Chemical Reaction Engineering and Technology, Department of Chemical Engineering, Tsinghua University, Beijing, 100084, P.R. China. E-mail: qianwz@tsinghua.edu.cn

Electronic Supplementary Information (ESI) available: [details of any supplementary information available should be included here]. See DOI: 10.1039/x0xx00000x

After quasi-solid-state crystallization treatment of the seeded MS spheres, the MFI zeolite structure was obtained (Fig. 1c). Almost all of the products presented the discrete and intact spherical morphology, and the original zeolite seeds on the MS surface grew to coffin-shaped crystals (Fig. 1e). The sizes of MFI zeolite were somewhat larger than that of the initial MS spheres, due to the outward oriented growth of zeolite during the MS transformation process. What was interesting for the present product was that the outer surface of zeolite sphere was composed of well-aligned c-axis oriented zeolite arrays perpendicular to sphere surface (Fig. 1f), like the bayberry (Fig. 1d). Seen from its cross-section by intentionally crushing (Fig. 1g), the product had a shell with 1−1.5 μm in thickness in the middle section and numerous NWs with length of 0.5−0.7 μm growing outside and inside the shell. The high density of c-axis oriented MFI crystals bonded by the middle layer ensured their structural stability. Since Si sources of MFI zeolite all came from the MS sphere, the growth of numerous ZSM-5 NWs consumed the solid core of MS spheres. Further chemical analysis was carried out using an EDS detector. The elemental maps of Si, Al and O (Fig. 1h−k) showed homogeneous distributions in the whole hollow structure.

TEM image showed that the diameter of NWs was about 0.2−0.3 μm (Fig. 1l). HRTEM characterization indicated that a lattice spacing of 1.3 nm was associated to the (001) lattice plane of MFI zeolite,[12,13] validating the NWs were single crystal and all c-axis oriented (Fig. 1m).

The well-ordered c-axis oriented MFI structure with various Si/Al ratios can also be synthesized under the similar synthetic conditions (Fig. S3 and Table S1). XRD patterns showed that all of samples with different Si/Al ratios possess highly crystalline MFI structure (Fig. 2a). We stressed here that the use of $NaAlO_2$ as mineralizer was the key to obtain such low Si/Al ratio of MFI zeolite. It was significantly better than the conventional mineralizer of NaOH, which was unable to prepare bayberry-shaped MFI zeolite with Si/Al ratio lower than 30, since the strong basicity of NaOH made the structure collapse.

Ar physisorption test confirmed that the surface area and pore structure of bayberry-shaped MFI zeolite were both different from that of pure micro- and nanosized zeolites (Table S1). The surface area was about 442−455 m^2/g, larger than that (423 m^2/g) of microcrystal, but smaller than that (484 m^2/g) of ZSM-5 nanoparticles (NPs). The middle value of surface area was reasonable since the bayberry-shaped MFI zeolite was composed of micrometer-thick shell and numerous ZSM-5 NWs. In addition, pore size distribution confirmed that there was not only micropores (centered at 0.55 nm) (Fig. 2b), but also mesopores at 2−10 nm (Fig. 2c), ascribed to the slit pores of neighboring NWs.

The ^{29}Si MAS NMR spectra (Fig. 2d) showed three resonance at −117, −113 and −107 ppm, respectively, after spectral deconvolution. The resonances at around −113 and −107 ppm were associated with the Si(0Al)(Q^4) and Si(3Si, 1Al) species, respectively, while the signal at −117 ppm was attributed to the crystallographically inequivalent Si(0Al) (Q^4) sites.[14,15] There were no resonances with chemical shifts below

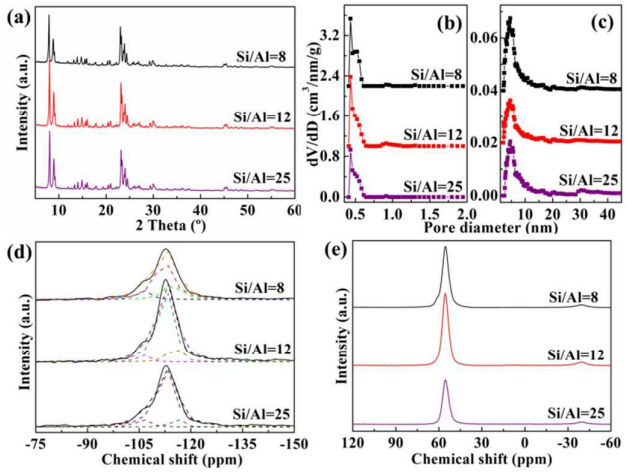

Fig. 2 (a) XRD patterns, (b and c) NLDFT pore size distributions, (d) ^{29}Si NMR, and (e) ^{27}Al NMR of the bayberry-like MFI zeolite with various Si/Al ratios.

100 ppm representing Si(2Si,2Al) sites in either of the samples, indicating that (Al-O-Si-O-Al) sequences were not present in these samples.[16] The ^{27}Al MAS NMR spectrum (Fig. 2e) of bayberry-like MFI zeolite showed one sharp aluminum peak at 55 ppm, indicating that all aluminum atoms were incorporated into the MFI framework with tetrahedral coordination environment.[14,15]

It was worth noting that the intact spherical morphology of MFI zeolite can be well retained even after calcination (in air, 1000 °C, 2h) and sonication (HF frequency) 50kHz, 100W, 1h) treatment (Fig. S4), implying the good thermal and mechanical stability of the products.

To study the crystallization process for the MFI zeolite systematically, the SEM images of the product at various hydrothermal stages were investigated. After hydrothermal heating for 2 hrs, the sphere surface showed no sign of crystallization (Fig. S5a and b), which was consistent with the XRD patterns that showed no detectable crystalline phase (Fig. 3e). After crystallization for 5 hrs, the low diffraction peaks of MFI topology appeared. The SEM images (Fig. 3a and b, Fig. S5c) and TEM images (Fig. 3c and d) taken from the edge of shell showed that MFI framework composed of countless needle−like nanocrystalline with the length of 300−500 nm and the diameter of 50−80 nm was formed firstly by consuming part of the MS spheres. The initially grown MFI zeolites were attached on the surface of MS spheres with c-axis perpendicular to the sphere surface. At 10 hrs, the length and the diameter were 500−800 nm and 200 nm, respectively (Fig. 3f and g, Fig. S5d), indicating that MFI zeolite grew both in axial and radial direction with the crystallization reactions going on. Although the morphology of external NWs changed insignificant from 10−24 hrs (Fig. 1e and f), the diffraction peak intensity was sustainably increased till to 24 hrs (Fig. 3e). It suggested that the crystallization did not occur homogeneously throughout the silica sphere, but preferably at the surface first, which was confirmed by the cross-sectional view (Fig. 3h−j) and the Ar isotherms at different crystallization times (Fig. S6, Table S2).

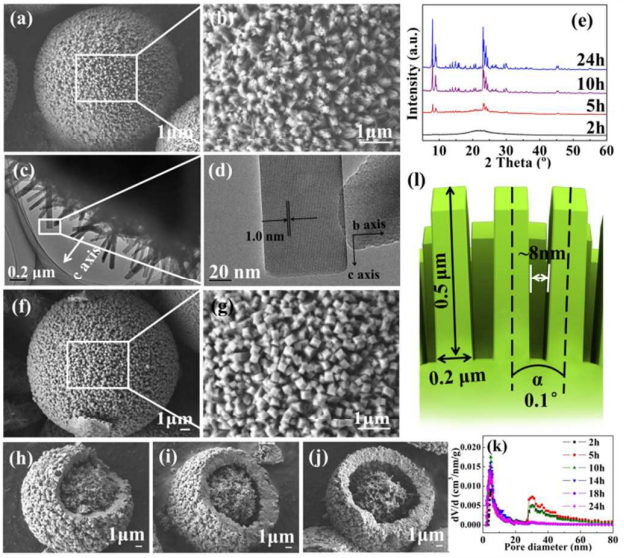

Fig. 3 Investigation on bayberry-like MFI zeolite crystallization. SEM images of sample crystallized at (a and b) 5h, (f and g) 10h; SEM images of the crushed sample at (h) 10h, (i) 14h, (j) 18h; (c and d) TEM images of sample crystallized at 5h; (e) XRD patterns of sample obtained at different crystallization times; (k) NLDFT pore size distributions at various crystallization stages; (l) Schematic diagram of the surface of c-axis oriented MFI zeolite.

To understand this, we crushed the hollow sphere crystallized at different times. After 10 hrs (Fig. 3h), it can be found that the silica sphere surface was covered with MFI crystals shell of ~1.5 μm in thickness, but the inner side was still amorphous. When the crystallization was further prolonged to 14 h, the silica sphere was converted into typical yolk-shell sphere (Fig. 3i), displaying a large void space between the unusual amorphous core and the c-axis oriented MFI shell. After reaction for 18 h, more amorphous silica was transformed into MFI crystals, and the voids became more obvious in the core part as a result of condensation and crystallization (Fig. 3j). The slow crystallization inside was easily understood considering the mass transfer barrier of steam from outside to inside the shell. The migration of Si species allowed the continuous growth inside the MFI middle layer, until the whole MS spheres were consumed after 24 hrs, leading to a bayberry-shaped MFI network (Fig. 1g). The flat baseline and high intensity of MFI diffraction peaks (Fig. 3e) confirmed the highly crystallized shells and the disappearance of the amorphous MS cores.

A much broad pore size distribution between 30 and 50 nm was observed before 10 hrs, while a steep increase of the cumulative pore volume in a pore size range of 2-10 nm was formed after 10 hrs (Fig. 3k and Table S2). The formation of this unusual bayberry-shaped structure with ~8 nm intervals between zeolites was dependent on the initial density of silicalite-1 nanoseeds locating on MS sphere surface. According to geometry, this bayberry-shaped structure with uniform size of ~16 μm in diameter exhibited 0.1° angle and ~8 nm intervals between two adjacent zeolites (Fig. 3l), which can be confirmed by Ar physisorption results (Fig. 3k).

The well-defined structure allowed us, for the first time, to calculate the weight ratio of NWs section to microsized shell section of bayberry-like zeolite. About 1.17×10^4 and 1.02×10^4 NWs (0.2 μm in diameter, 0.5 μm in length) grew outside and inside the shell (1.2 μm), respectively, if growing densely was like that in Fig. 3l. The weight ratio of all NWs to microsized shell was about 1:2. Apparent, bayberry-like zeolite prepared here was a structure combing nano- and micro- crystals.

Through an *in-situ* crystallization process,[17-19] the unique bayberry-like MFI zeolite containing well-dispersed uniform ZnO NPs was synthesized with good structural stability. During the quasi-solid-state crystallization process, ZnO NPs did not impact the c-axis oriented growth of zeolite crystals, resulting in bayberry-shaped ZnO/MFI zeolite (Fig. S7a and b). The cross-section SEM image (Fig. S7c) and the XRD patterns (Fig. S8) revealed that the ZnO/MFI zeolite had a high crystallinity and the whole amorphous MS spheres were consumed. The elemental maps of Si, Al, O and Zn (Fig. S7f–i) showed homogeneous dispersions in the whole structure. There was no diffraction peak of ZnO in XRD patterns (Fig. S8), and the ZnO NPs were also not observed in TEM images (Fig. S7d and e). Combined with the EDS results (Fig. S7h), it can be speculated that the ZnO were highly dispersed in MFI zeolite, which were preferable for heterogeneous catalysis, e.g., the MTA reaction.

As follows, the catalytic performances of bayberry-like ZnO/ZSM-5 were compared with the conventional microsized ZSM-5 (Si/Al=25) and ZSM-5 NPs (Si/Al=25), both doped with ZnO, in a fixed bed stainless steel reactor. Catalyst based on ZSM-5 NPs exhibited the longest lifetime (Fig. 4a). It endured 7 hrs when the conversion of methanol was always higher than 97%. Catalyst based on microsized ZSM-5, however, only endures 2.5 hrs before the conversion of methanol is lower than 95%. The great difference was attributed to the small size of NPs which had excellent diffusion channel for large molecules out of the matrix. Bayberry-like ZnO/ZSM-5 exhibited a middle lifetime between them and was

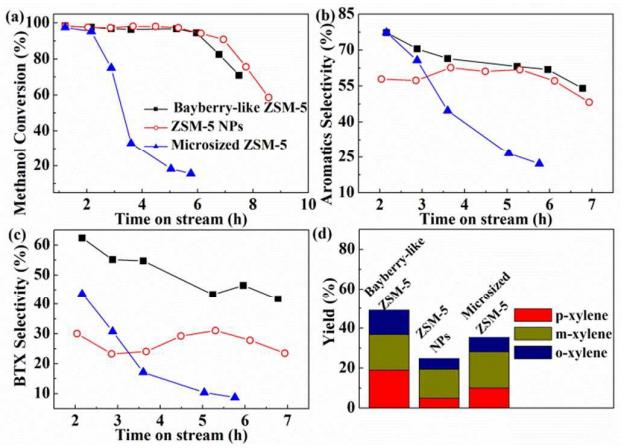

Fig. 4 Comparison of the catalytic performance of bayberry-like MFI zeolite with microsized ZSM-5 and ZSM-5 NPs in MTA reaction. (a) Methanol conversions, (b) total aromatics selectivity, (c) BTX selectivity, (d) Yield of xylene with time on stream (reaction temperature: 475°C, WHSV: 0.75 h^{-1}).

much close to the ZSM-5 NPs in the initial 6.5 hour reaction. On the other hand, bayberry-like ZnO/ZSM-5 exhibited much higher aromatic selectivity (the selectivity of B, T, X and TriMB etc.) than ZnO/ZSM-5 NPs, since the former had lower Si/Al ratio (Fig. 4b). The decreasing trends of aromatics selectivity with the time over bayberry-like ZnO/ZSM-5 was slightly quick than that over ZnO/ZSM-5 NPs, but was much slower than that over ZSM-5 microcrystals, due to their excellent diffusion property.

In detail, the selectivity of BTX in all aromatics, over bayberry-like ZnO/ZSM-5, was the highest among three catalysts (Fig. 4c). The value approached to 64% at 2hrs, 1.5 times that over microsized catalyst and 2.2 times that over nanosized catalyst. The value was still higher than 47% even after the continuous reaction of 6 hrs. In sharp contrast, the value dropped from 43% at 2 hrs quickly to 17% at 3.6 hrs, over the microsized catalyst. Apparent, the easy coke deposition over microsized catalyst weakened its acidity and accelerated the alkylation of X to tri- or tetra-methylbenzene in the final stage of the reaction (>4 hrs). On the other hand, BTX selectivity over nanosized catalyst nearly didn't drop at 6 hrs, confirming its very excellent diffusion ability to give the lowest coke deposition rate. However, the value was very low and never exceeded 30%. It was attributed to the huge external surface, resulting in too rapid alkylation of X. In the literatures previously, Ni et al[20,21] and Shen et al[4] have investigated the catalytic performance of ZSM-5 catalysts in MTA reaction, which was found to be obviously lower than that over the bayberry-like MFI zeolite in our study (Table S3 and Table S4). As shown in Fig. 4d, the yield of X or PX over bayberry-like ZnO/ZSM-5 was much higher than the microsized catalyst and ZnO/ZSM-5 NPs (X Yield = Methanol conversion × X selectivity). Among product of B, T, X and tri- or tetra-methylbenzene worldwide, the demanded amount of X, especially PX, as well as its price, was the highest.[2,3] Therefore, bayberry-like ZSM-5 gave a higher-value product with high yield, thanking to the synergistic effect between NWs and microsized shell. Other products and their distribution were shown in Table S5.

Because this integrated structure contained nanosized-sections and microsized-sections with suitable ratios, and the nanosized MFI crystals bonded by the middle microsized layer ensured their structural stability, this special structures was effective to avoid the aggregation of nanoparitcles as directly packed in reactor, and to avoid the rapid deactivation of microsized crystals by coke deposition,[22,23] and to avid the low efficiency of large-size molded catalyst particles composed of much components (adhesive binder or mechanical filler) not contributing to the activity.[24,25] It is the first structure combining both the advantages and avoiding both the disadvantages of the microsized and nanosized crystals.

In conclusion, we have successfully synthesized bayberry-shaped MFI zeolite with micrometer-thick shell and numerous c-axis oriented NWs outside and inside the shell through quasi-solid-state crystallization approach. The bayberry-like ZSM-5 had both the middle value of BET surface area and pore size distribution between that of microcrystal and nanocyrystals. Consequently, it exhibited a higher conversion of methanol, longer lifetime of the catalyst, compared to that over ZSM-5 microcrystals. It also gave a better aromatic product distribution than that over pure nanocrystals. It confirmed the advantage of hierarchical structure with rational ratios of micro to nanosections for heterogeneous reactions, compared to the pure microcrystal and nanocrystals.

Notes and references

1 K. Shen, W. Qian, N. Wang, C. Su and F. Wei, *J. Am. Chem. Soc.,* 2013, **135**, 15322−15325.
2 J. Zhang, W. Qian, C. Kong and F. Wei, *ACS Catal.,* 2015, **5**, 2982−2988.
3 J. Zhang, W. Qian, X. Tang, K. Shen, T. Wang, X. Huang and F. Wei, *Acta Phys. Chim. Sin.*, 2013, **29**, 1281−1288.
4 K. Shen, W. Qian, N. Wang, C. Su and F. Wei, *J. Mater. Chem. A,* 2014, **2**, 19797–19808.
5 K. Shen, N. Wang, W. Qian, Y. Cui and F. Wei, *Catal. Sci. Technol.,* 2014, **4**, 3840–3844.
6 W. Song, R. Kanthasamy, V. H. Grassian and S. C. Larsen, *Chem. Commun.,* 2004, 1920–1921.
7 Z. Sun, Y. Zhang, X. Deng, J. Li and C. Xiong, *J. Ind. Eng. Chem*., 2012, **18**, 92–97.
8 J. Hua and Y. Han, *Chem. Mater.,* 2009, **21**, 2344–2348.
9 W. Fan, M. A. Snyder, S. Kumar, P. S. Lee, W. C. Yoo, A. V. McCormick, R. L. Penn, A. Stein and M. Tsapatsis, *Nat. Mater.,* 2008, **7**, 984–991.
10 N. Wang, K. Shen, X. Yu, W. Qian and W. Chu, *Catal. Sci. Technol.,* 2013, **3**, 2278–2287.
11 D. Xu, Z. Jing, F. Cao, H. Sun and S. Che, *Chem. Mater.,* 2014, **26**, 4612–4619.
12 K. Na, C. Jo, J. Kim, K. Cho, J. Jung, Y. Seo, R. J. Messinger, B. F. Chmelka and R. Ryoo, *Science,* 2011, **333**, 328–332.
13 F. Liu, T. Willhammar, L. Wang, L. Zhu, Q. Sun, X. Meng, W. Carrillo-Cabrera, X. Zou and F. S. Xiao, *J. Am. Chem. Soc.,* 2012, **134**, 4557−4560.
14 P. Sazama, J. Dedecek, V. Gabova, B. Wichterlova, G. Spoto and S. Bordiga, *J. Catal.,* 2008, **254**, 180–189.
15 Z. Wan, W. Wu, W. Chen, H. Yang and D. Zhang, *Ind. Eng. Chem. Res.,* 2014, **53**, 19471−19478.
16 L. Huang, Z. Wang, J. Sun, L. Miao, Q. Li, Y. Yan and D. Zhao, *J. Am. Chem. Soc.,* 2000, **122**, 3530–3531.
17 C. H. Christensen, I. Schmidt, A. Carlsson, K. Johannsen and K. Herbst, *J. Am. Chem. Soc.,* 2005, **127**, 8098−8102.
18 M. Choi, Z. Wu and E. Iglesia, *J. Am. Chem. Soc.,* 2010, **132**, 9129–9137.
19 B. Li, B. Sun, X. Qian, W. Li, Z. Wu, Z. Sun, M. Qiao, M. Duke and D. Zhao, *J. Am. Chem. Soc.,* 2013, **135**, 1181−1184.
20 Y. Ni, W. Peng, A. Sun, W. Mo, J. Hu, T. Li and G. Li, *J. Ind. Eng. Chem.,* 2010, **16**, 503–505.
21 Y. Ni, A. Sun, X. Wu, G. Hai, J. Hu, T. Li and G. Li, *Microporous Mesoporous Mater.,* 2011, **143**, 435–442.
22 K. Möller and T. Bein, *Chem. Soc. Rev.*, 2013, **42**, 3689-3707.
23 W. J. Roth, P. Nachtigall, R. E. Morris and J. Čejka, *Chem. Rev.,* 2014, **114**, 4807–4837.
24 K. Okada, K. Kuboyama, T. Takei, Y. Kameshima, A. Yasumori and M. Yoshimura, *Microporous Mesoporous Mater.,* 2000, **37**, 99–105.
25 A. Jakob, V. Valtchev, M. Soulard and D. Faye, *Ind. Eng. Chem. Res.,* 2010, **49**, 5616–5624.

